HORIZON EUROPE PROGRAMME
TOPIC HORIZON-CL5-2023-D3-01-02

GA No. 101136094

Sustainable Photovoltaics Integration in buildings and Infrastructure for multiple applications

SPHINX - Deliverable report

D3.4 – Advantages of matrix shingle technology for integrated PV

Funded by
the European Union

Deliverable No.	D3.4	
Related WP	WP3	
Deliverable Title	Advantages of matrix shingle technology for integrated PV	
Deliverable Date	Officially planned Feb 2024, extension requested till June 2024	
Deliverable Type	Report	
Dissemination level	PU	
Author(s)	Torsten Rößler (Fraunhofer), Frank Ennslen (Fraunhofer), Daniel von Kutzleben (Fraunhofer), Elmar Lohmüller (Fraunhofer), Jale Schneider (Fraunhofer), Johannes Greulich (Fraunhofer), Nils Klasen (M10 Industries), Florian Jean-Christophe Ollagnon (EPFL)	
Checked by	Jacques Levrat (CSEM), Laurianne Wendling (VOL), Antonin Faes (EPFL)	
Reviewed by (if applicable)	Jacques Levrat (CSEM)	11-06-24
Approved by	Laurianne Wendling (VOL)	13-06-24
Status	Final	

Document History

Version	Date	Editing done by	Remarks
V1	April 2024	Fraunhofer, UNR	First version
V2/Final	June 2024	Fraunhofer, UNR, VOL, CSEM	Final version

Public Summary

The SPHINX project, funded by the EU's Horizon Europe programme, focuses on advancing matrix shingle technology for integrated photovoltaic (PV) applications. This innovative technology enhances the efficiency, shading resilience, and integration flexibility of PV modules, making them ideal for building integrated applications.

Matrix shingle technology involves cutting full wafer solar cells into narrow strips called shingles, which are interconnected using electrically conductive adhesives (ECA) in a brickwall pattern. This method eliminates the need for traditional interconnector wires, maximizing the active photovoltaic area within the module and providing a uniform, aesthetically pleasing appearance. Thermal Laser Separation (TLS) is employed for cell cutting with minimal damage, thereby reducing efficiency losses due to edge recombination. Post-cutting, the edges of the shingles are passivated using aluminum oxide (Al_2O_3), deposited through high-throughput plasma-enhanced atomic layer deposition (PE-ALD). This process significantly reduces charge carrier recombination at the cell edges, enhancing cell efficiency.

The matrix design distributes current generation across the module surface, making it more resilient to partial shading. Unlike traditional modules that can suffer significant power losses from shading, matrix shingle modules maintain higher energy output under similar conditions. ECAs used in matrix shingle technology provide both electrical connectivity and mechanical adhesion. These lead-free, flexible polymeric materials filled with conductive particles ensure robust interconnections that can withstand mechanical stresses and environmental conditions.

Applications of matrix shingle technology include building-integrated photovoltaics (BIPV), vehicle-integrated photovoltaics (VIPV), and agrivoltaics (AV). In BIPV, the flexible design allows seamless integration into building facades and roofs, maximizing energy generation while enhancing architectural aesthetics. In VIPV, the technology supports customized solar module placement on vehicles, optimizing energy generation without compromising design. For AV, matrix shingle technology enables dual land use by generating electricity and enhancing crop yield through customizable light transmission patterns.

The Fraunhofer ISE pilot production line supports the scalable manufacturing of matrix shingle modules, facilitating the transition from prototype development to large-scale production. This ensures that these advanced PV modules can be effectively integrated into various applications, driving sustainable energy solutions across multiple sectors.

Content

List of Figures

List of Tables

Abbreviations & Definitions

Abbreviation	Explanation
AGV	Automated Guided Vehicle
AI	Artificial Intelligence
AV	Agrivoltaics
BIPV	Building-Integrated Photovoltaics
CAGR	Compound Annual Growth Rate
DH	Damp Heat
ECA	Electrically conductive adhesive
EL	Electroluminescence
IPV	Integrated Photovoltaics
IV	Current-Voltage
LDC	Laser direct cleaving
LSMC	Laser Scribe and Mechanical Cleaving
ML	Mechanical load
Module-TEC	Module Technology Evaluation center
PE-ALD	Plasma enhanced atomic layer deposition
PERC	Passivated emitted rear contact
PET	Passivated edge technology
PV	Photovoltaics
SHJ	Silicon-heterojunction
T-ALD	Thermal Atomic Layer Deposition
TC	Thermal Cycling
TLS	Thermal Laser Separation
TOPCon	Tunnel Oxide Passivated Contact
VIPV	Vehicle Integrated Photovoltaics
W_p	Watt-peak

1 Introduction

1.1 Integrated Photovoltaics

Integrated Photovoltaics (PV) refers to the incorporation of solar cells into building materials or structures, enabling them to generate electricity while serving their primary purpose (Belle, 2016). This approach seamlessly integrates renewable energy generation into the built environment, offering numerous benefits such as energy efficiency, sustainability, and aesthetics (Kuhn, 2021).

The integrated PV market has experienced substantial growth in recent years, with the global market size projected to reach around USD 143.99 billion by 2032, expanding at a remarkable compound annual growth rate (CAGR) of 22.5% (IMARC, 2023). This growth trajectory is fuelled by a surge in demand for sustainable building solutions, coupled with government incentives promoting renewable energy adoption (IMARC, 2023; The Business Research Company, 2023). Moreover, advancements in technology and cost reductions have further catalysed market expansion, making integrated PV solutions increasingly accessible and attractive to consumers (IMARC, 2024). Analysts foresee continued growth in the coming years, driven by heightened environmental awareness and stringent regulatory requirements for energy-efficient construction practices adoption (IMARC, 2023; The Business Research Company, 2023). These factors collectively underscore the significant momentum behind the integrated PV market, highlighting its pivotal role in the transition towards a more sustainable and renewable energy-driven future.

Key requirements for the integrated PV market include improved efficiency, durability, and architectural integration. Current products range from solar roof tiles to facade-integrated PV modules. While these offerings provide renewable energy generation, challenges remain in optimising performance, enhancing durability, and reducing installation costs. Innovations in materials and manufacturing processes are driving product improvements, addressing these market needs.

Future advancements in integrated PV technologies aim to enhance efficiency, flexibility, and cost-effectiveness. Research focuses on developing high-performance solar materials, innovative installation methods, and smart integration solutions. By addressing these areas, manufacturers can deliver more efficient and aesthetically pleasing integrated PV products, further driving market adoption.

As the drive for innovation propels the integrated PV market forward, there is a growing demand for transformative solutions that not only enhance efficiency and flexibility but also address the evolving needs of diverse applications. Among these emerging technologies, matrix shingle technology stands out as a pioneering approach that offers unique advantages for integrated PV applications. By leveraging innovative design principles and material advancements, matrix shingle technology presents a promising avenue to overcome existing challenges and unlock new possibilities in numerous IPV domains as presented in the subsections below.

1.1.1 Building-Integrated Photovoltaics (BIPV)

Matrix shingle technology provides a cost-effective and aesthetically pleasing solution for BIPV applications, meeting both energy efficiency and architectural design requirements, e.g., homogeneous appearance. The high flexibility in size and dimensions makes roof corners and window recesses or facade projections particularly easy to accommodate. The possibility of alternating cells in a chess-pattern to play with module transparency allows to enhance building aesthetics while

generating electricity. With its flexible and modular design, matrix shingle technology also facilitates the integration of PV modules into building facades, maximizing energy generation potential. Its intrinsic resilience to partial shading is particularly suited for facade having static or recurring shading events, improving energy yield, but also safety.

1.1.2 Vehicle-Integrated Photovoltaics (VIPV)

Matrix shingle technology offers a compelling solution for VIPV due to its flexible characteristics. These properties enable seamless integration of solar panels into vehicles. The high flexibility of matrix shingle technology allows for customization in sizes and shapes, aligning perfectly with the unique design constraints of vehicles. This adaptability is especially beneficial for car integration, where active areas are limited by windows and curvatures. By leveraging matrix shingle technology, manufacturers can optimize solar panel placement on vehicles, maximizing energy generation while maintaining aerodynamics and aesthetics.

1.1.3 Agrivoltaics (AV)

Integrating solar technology into agricultural areas, like greenhouses or open fields, serves the dual purpose of enhancing crop yield and generating electricity. This innovative approach offers significant market potential and addresses both agricultural and technological needs. To optimize this dual use, solar panels must be translucent and adaptable to meet the specific irradiance requirements of different crops. Matrix shingle technology provides an excellent solution for this, allowing for customizable light transmission by adjusting shingle elements in various patterns, such as chess patterns or spaced strings.

IPV represent a promising approach to sustainable energy generation in the built environment. With advancements in technology and increasing market demand, the integration of solar cells into building materials is expected to continue its growth trajectory. Matrix shingle technology, with its innovative design and numerous advantages, is well-positioned to drive further adoption across various integrated PV applications.

1.2 Mainstream Photovoltaic Module Technology

A solar module, also known as a photovoltaic module, is a device composed of multiple interconnected solar cells to increase the overall output voltage. A state-of-the-art solar module is shown Figure 1a. Furthermore, the structure of the solar module is shown in Figure 1b. The solar cells are encapsulated to be protected against environmental conditions, ensuring operational efficiency and durability. The encapsulation employs highly transparent, elastomeric polymers, typically ethylene-vinyl acetate or polyolefins. The module's external protection consists of transparent, low-iron glass, and the rear is secured by either an additional glass pane or a robust, polymer-based back sheet. Additionally, the module incorporates one or more junction boxes housing bypass diodes, and is framed with aluminium along the glass edges for enhanced structural integrity. A typical production sequence of a solar module is shown in Figure 2. Optimizing the specific production costs — by either enhancing power output with minimal costs or lowering the costs while preserving power output — alongside guaranteeing a stable power output for a minimum of 25 years, are crucial objectives in PV module manufacturing.

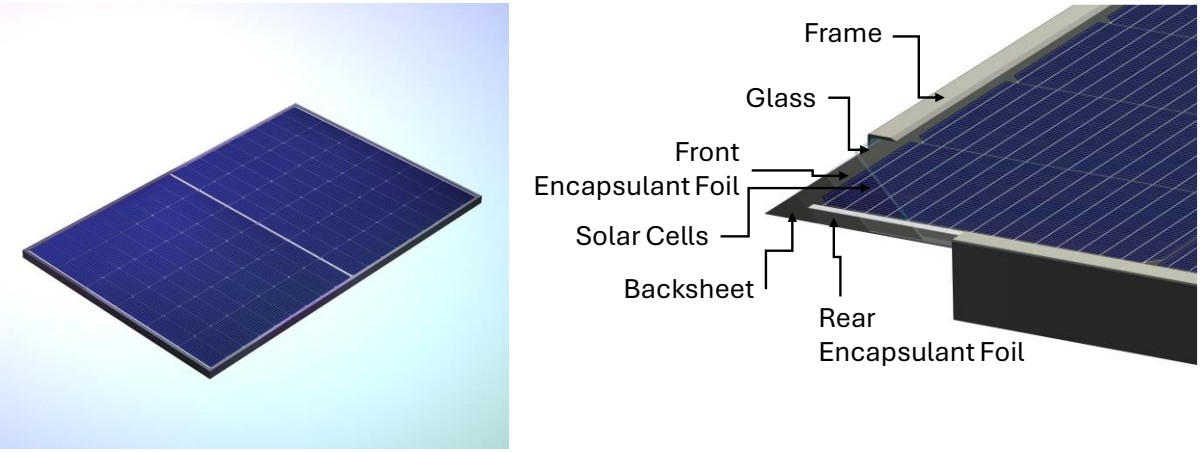

Figure 1: a) Front view of a mainstream solar panel with solar cells in half-cut format interconnected with 16 wires. The module is 1.1 m wide and 1.7 m long, b) Cross section of the solar module showing the individual components

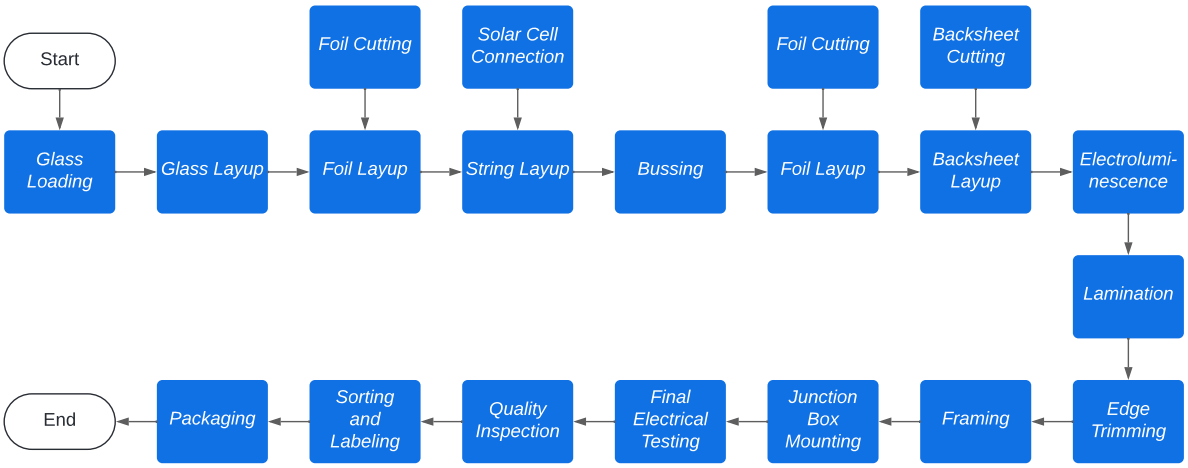

Figure 2: Process flow of a module production process, adapted from Wirth (2020).

In the last decades, a drastic increase in innovation occurred in the PV industry. Global warming, energy crisis and the increase in electricity price have driven this trend. Therefore, new technologies have developed in the market. Passivated emitted rear contact (PERC) cells represent the biggest marker share (~80%). However, new emerging technologies are expected to dominate the market in the future. Silicon-heterojunction (SHJ) and tunnel oxide passivated contact (TOPCon) cells are believed to represent respectively 25% and 60% of the market share in 2033 adoption (VDMA, 2024).

Since the first commercially available solar panels, a considerable drop in prices have been observed. Indeed, as shown in Figure 3(a), the price per Watt-peak Wp decreased from 125.8 $ to 0.25 $ in roughly 50 years adoption (IRENA, 2023), rendering solar energy more attractive. This reduction is due to multiple factors such as the increase in efficiency while reducing the quantity of materials needed at both the cell and module level. These elements are accompanied by the increase in production, also observed on Figure 3(a), which allows economies of scale, decreasing the price per unit adoption (Kavlak et al., 2018). In turn, the attractiveness of low-cost solar energy increases the demand and thus expands the supply. Therefore, the reduction in costs and the increase in capacity affect each other in a virtuous circle, from an energy transition perspective.

In addition, with the decrease of module price per Wp, a wider range of applications becomes attractive. As shown in the previous section, multiple fields of installations are emerging such as

agrivolatics (AV), vehicle integrated photovoltaics (VIPV) and building-integrated photovoltaics (BIPV), increasing the effective area available for solar panels without affecting the land use.

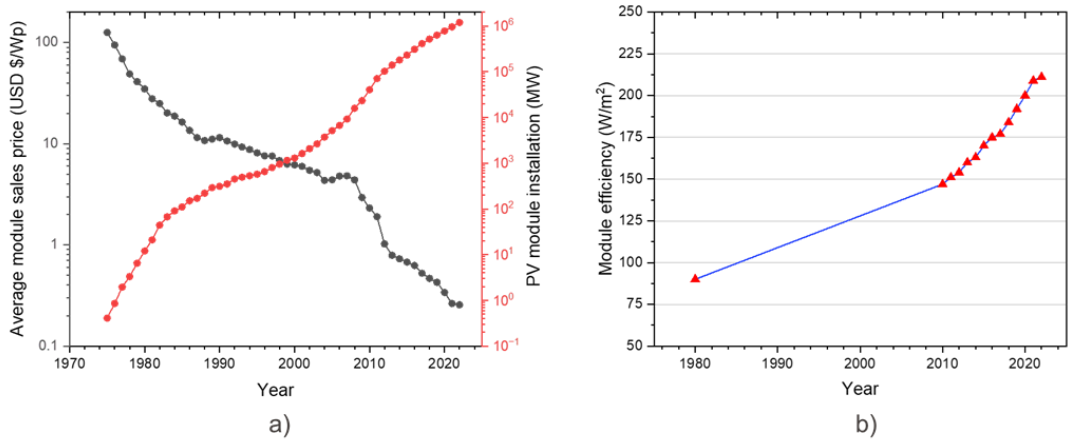

Figure 3: (a) The cost of PV module and the accumulative PV installation since 1975. Data obtained from Statista (2023), IRENA (2023), VDMA (2023). (b) Module efficiency evolution since 1980 based on the average module efficiency before 2010 and on PERC-type module after. Data taken from VDMA (2022, 2021, 2020, 2019, 2018, 2017, 2016, 2015, 2014, 2013, 2012, 2011).

Module efficiency can be defined as the maximum power output per area of a solar module at 25 °C under 1000 W/m^2 irradiance with AM1.5 spectrum. It can be expressed either in W/m^2 or in percentage (divided by the irradiance). In this report, the module efficiency will be presented in W/m^2 as matrix shingling aims for a high output per area. In Figure 3(b), the increase of module efficiency over time is shown. To simplify calculations, the efficiency is based on the average cell technologies used in modules before PERC cells entered the market around 2010, and on PERC type modules after 2010 (Green, 2015). The latter assumption was done because PERC cells represent the biggest market share at the time of writing (VDMA, 2023). One can observe the increase from 90 to 211.1 W/m^2 power output. This rise derives logically from the increase in solar cell efficiency, but also from the cell size. Indeed, cells evolved from M0 to G12 size, with less surface loss in the corners and allowed gains in module efficiency of up to 77% (Mittag et al., 2020). Moreover, module materials such as encapsulants or the cover glass have also been optically optimized to allow more light into the cell, decreasing the cell to module loss (Allsopp et al., 2020).

The increase in cell size necessitated the use of more interconnectors per cell[1] to minimize series resistance losses caused by the interconnections. This trend was further accelerated by the need to reduce the silver content in cell metallization[2], which correlated with reduced metallization finger width[3].

To avoid overall losses, this reduced metallization must be contacted with more interconnectors. Consequently, the increasing number of interconnectors per cell has posed significant challenges for machines to handle numerous wires in parallel.

[1] The 15th edition of the ITRPV roadmap forecasts that by 2024, 50% of the annual production of solar cells will have more than 12 busbars or will be busbarless. This figure is expected to increase to 60% by 2026 and 90% by 2028 (VDMA, 2024).

[2] Currently, 115 mg of silver is used per cell in TOPCon solar cells. This amount is projected to decrease to 100 mg by 2026 and 90 mg by 2028 (VDMA, 2024).

[3] The current metallization finger width for solar cells is approximately 25 µm, and it is expected to be reduced to 20 µm by 2028 (VDMA, 2024).

Shingling is an excellent approach to keep the interconnection simple and flexible because no wires are required. Additionally, it supports the overall trend to obtain higher module efficiency at reduced costs. The main technological aspects and advantaged of matrix shingling will be shown in the next sections.

2 Matrix Shingle Technology

2.1 The Basic Concept

Shingling is an interconnection technology designed to increase module efficiency by maximizing the photovoltaic active area within the PV module. This technology also eliminates the need for interconnector wires. Currently, the market share of shingled PV modules is below 5% (VDMA, 2024). However, this market share is expected to grow due to the increasing demand for building-integrated photovoltaics. In this market, there is a high demand for aesthetically pleasing modules. Shingle interconnection of solar cells produces highly uniform PV modules, meeting these aesthetic requirements particularly well.

The basic concept of shingling involves the direct front-to-rear interconnection of solar cells (C. Dickson Jr., 1960). Currently, Sunpower/Maxeon offers shingled solar modules (“Performance series”) as commercial products (Sunpower/Maxeon, 2024). Other manufacturers, such as Tongwei and Solaria, have also offered these modules in the past. Various patents protecting intellectual property related to the production chain are in place, particularly in the US.

The process of shingling involves cutting full wafer solar cells into narrower cell stripes ("shingles") using a laser. Typical cutting ratios are 1/5, 1/6, 1/7, or 1/8 of the full cell, depending on the conductivity of the metallization and the additional loss created by the damage at the cell edge (Wöhrle et al., 2017). The solar stripes are slightly overlapped during the shingling process in the stringer, similar to roof tiles, with an overlap of around 1 mm.

The bond between two shingles is formed by a layer of electrically conductive adhesive (ECA) with a thickness of 10 µm to 50 µm, cured at temperatures below 180 °C. A schematic representation of the ECA in a shingle interconnection is shown Figure 5.The ECA facilitates both electrical conductivity and mechanical adhesion. These adhesives are lead-free polymeric materials filled with conductive particles, often silver, with filler content ranging between 40% wt and 80% wt (Schulte-Huxel et al., 2021; Geipel, 2017).

ECAs are relatively flexible, with Young’s moduli ranging from 100 MPa to 8000 MPa, allowing them to absorb mechanical stress (such as bending) effectively. Due to this property, ECAs are the preferred choice for directly attaching brittle silicon pieces in large devices that must withstand mechanical loads and other environmental stresses (Schulte-Huxel et al., 2021).

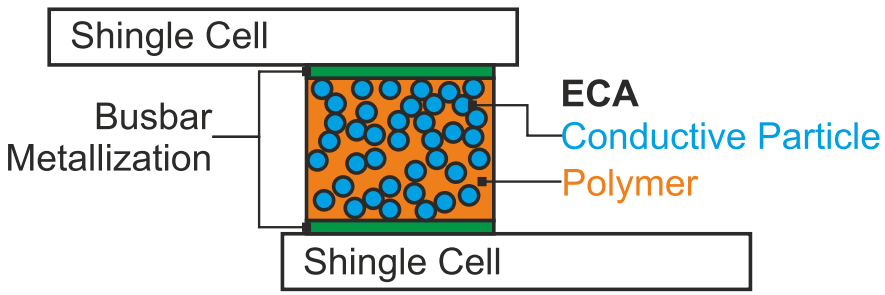

Figure 4: Description of the components of an electrically conductive adhesive in a shingle interconnection.

Shingled PV modules have the potential to yield higher efficiency than conventional PV modules (Huyeng et al., 2023; Rößler et al., 2022; Mittag et al., 2017). Key factors for achieving this advantage include a precise laser cutting process to minimize edge recombination (Münzer et al., 2020), effective

edge passivation (Lohmüller et al., 2023a), and reducing the shingle overlap to 0.5 mm (Tous et al., 2023).

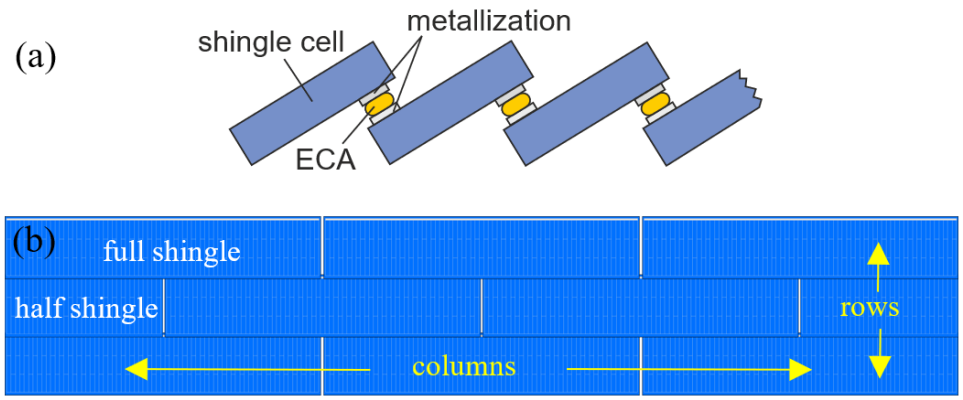

Figure 5: (a) Shingle interconnection of solar cells, depicting direct cell-to-cell interconnection along the cell edge with an overlap. The bond between shingles is formed by a layer of electrically conductive adhesive. (b) Matrix shingling, showing every second row of solar cells shifted laterally by half a shingle, creating a brickwall-like interconnection.

The concept of matrix shingling originated from Schmidt and Rasch in 1990 (Schmidt and Rasch, 1990). Fraunhofer ISE began upscaling the concept to full-format modules in 2018 (Mondon et al., 2018) and, in collaboration with M10 Industries, completed the development of industrial high-throughput equipment to produce these modules in 2022 (von Kutzleben et al., 2022). Matrix shingling is based on the principle of linear shingling, as depicted in Figure 5a, but incorporates an additional lateral offset in every second row by inserting half shingles in the outermost columns. This approach is similar to masonry wall construction. The result is a matrix of flexible length and width, where the shingles in each row are connected in parallel using the busbars of the overlapping cells, and the rows are connected in series with each other. A drawing of the matrix can be seen in Figure 5b, and a visualization of a full-format module is shown in Figure 6.

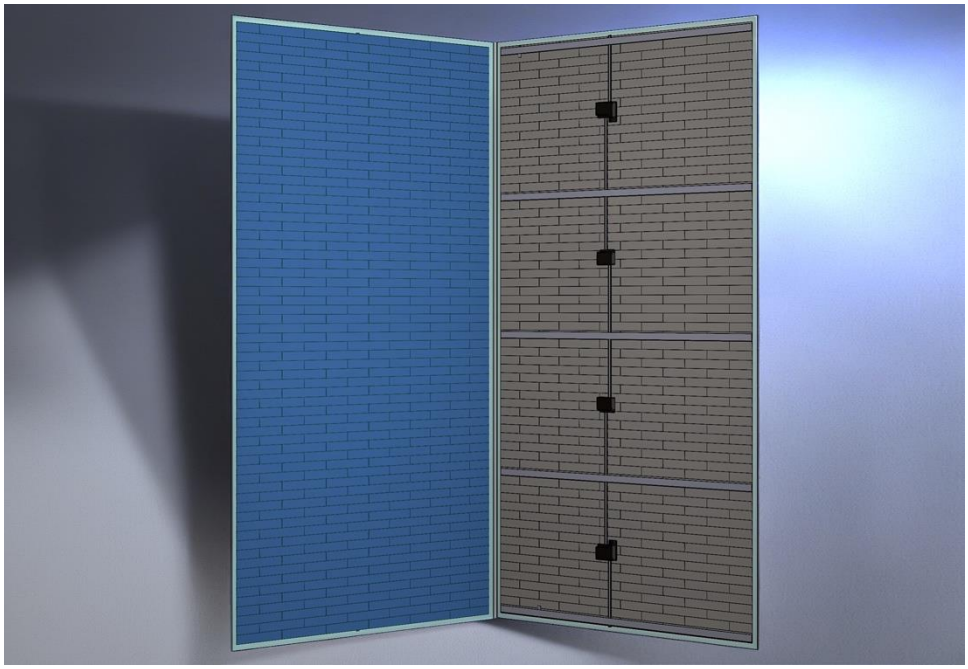

Figure 6: Visualisation of the front (left) and rear (right) sides of a full-format matrix shingle module.

2.2 Design Principles for Matrix Modules

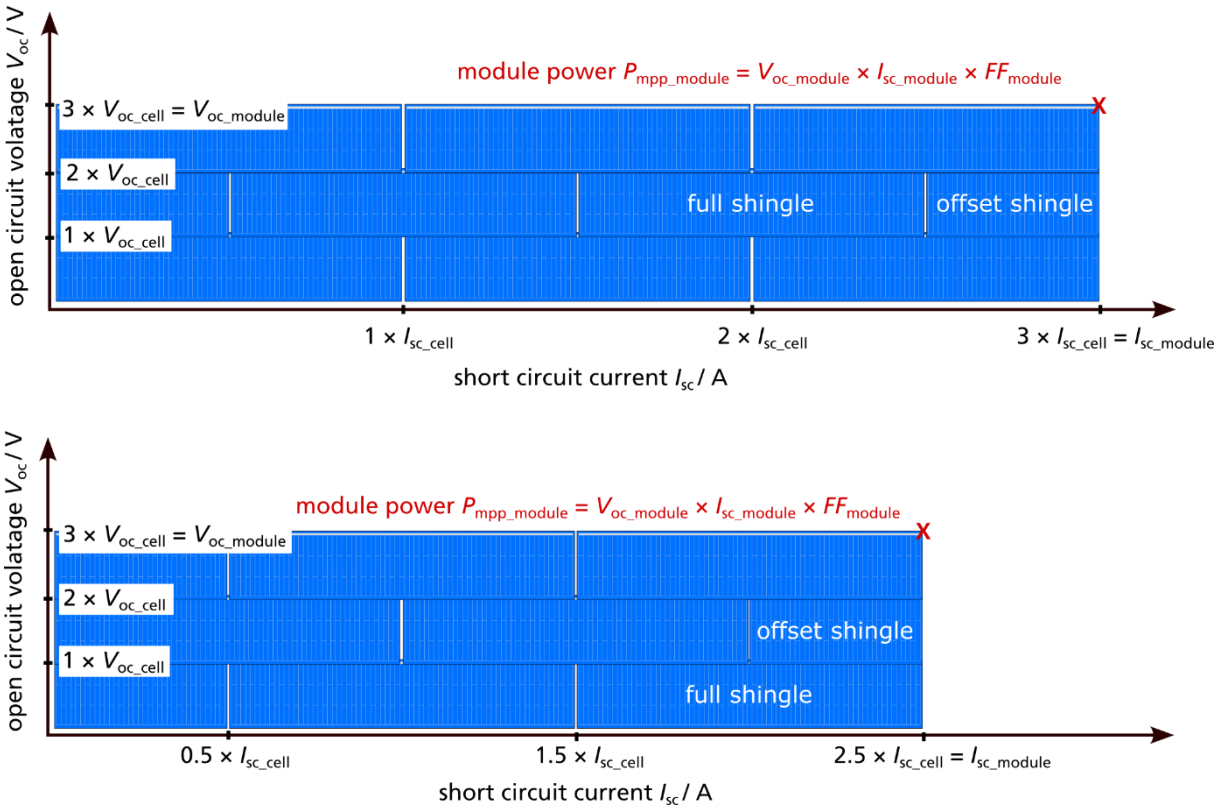

Figure 7: Drawing of two small matrix examples. (a) Matrix with three cell rows and three cell columns. (b) Matrix with three cell rows and two and a half cell columns. The current increases along the cell columns, and the voltage increases along the cell rows.

When designing a matrix module, the number of cells in series (cell rows) and the number of cells in parallel (cell columns) define the outer dimensions of the cell matrix within the module. The width of the matrix is determined by the shingle cell length (e.g., 210 mm for G12) multiplied by the number of columns, plus the size of the gap between the shingles (typically 0.5 mm) multiplied by the number of gaps. The length of the matrix is calculated by taking the shingle cell height (e.g., 26.25 mm for 1/8th of G12) multiplied by the number of rows, minus the cell overlap (e.g., 1.2 mm) multiplied by the number of cells overlaps (number of cell rows - 1). The offset shingles (see Figure 7) and their size (half, third, quarter, etc., of a full shingle) offer high flexibility in adjusting the width of the matrix. If the offset shingles are half the length of a full shingle, it is possible to have one offset shingle in every row of the matrix (Figure 7a), or two offset shingles in every second row (Figure 7b).

Figure 7 also explains how voltage, current and power are calculated for a given matrix. The current of the module is defined by the number of columns times the current of one cell, the voltage is obtained by the number of rows and the voltage of one cell. In order to calculate the module power PMPP, the short circuit current ISC of the module, the open circuit voltage VOC of the module and the fill factor (FF) of the module are multiplied. To finish the geometrical design one more cell row has to be added to enable the bussing as explained in section “Bussing and Diode Integration” and the side margins according to the voltage class of the module (e.g. 14.2 mm for 1000 V) (International Electrotechnical Commission, 2016). If the module is to have a frame, the last step must consider the frame geometry.

Adding frames usually increases the overall dimensions of the module by a few millimetres in each direction.

2.3 Partial Shading Resilience

It is important to differentiate between large area shading of a PV system, such as from dust, clouds, or snow, which can homogeneously lower the irradiation on a solar panel, and partial shading. Partial shading is caused by smaller objects directly on or near the solar panel, shading only parts of the surface and resulting in inhomogeneity in the spatial irradiation distribution. Examples include chimneys, antennas, bird droppings, leaves, nearby trees, or other buildings.

Due to the nature of the electrical series interconnection in solar panels, such partial shading events usually cause disproportionate power losses. Following the principles of current conservation, the currents in serial interconnections through all elements must match. Inhomogeneous irradiation causes different currents to be produced in the interconnected elements. This current mismatch is the root cause of the disproportionate power losses, because shaded elements limit the power output of their unshaded neighbors. These losses are a driving factor for yield losses in PV systems.

The Shingle Matrix Technology has properties that mitigate the impact of partial shading on power and, consequently, yield. In principle, they all lead to a reduction in current mismatch.

2.4 Beneficial Properties of the Shingle Matrix Technology

2.4.1 Distributed Current Generation

To achieve similar voltage-current characteristics, module layouts for shingle interconnections implement parallel interconnections to compensate for the low currents produced by the smaller shingle solar cells. Consequently, the overall module current is spatially distributed across the surface of the PV panel, unlike in panels with full-square solar cells (Figure 8). In the latter case, a relatively small random shade can cover an entire full-square solar cell in panel A, thereby reducing the current to zero. However, the same shade (black rectangle) cannot cause the same effect in panels B and C, where current generation occurs in the two parallel interconnected blocks and six parallel interconnected columns, respectively. It is important to note that in both panels B and C, many other combinations of solar cells in each parallel interconnected substring would reduce the current to zero, but a larger shade than the black rectangle would be required in all cases.

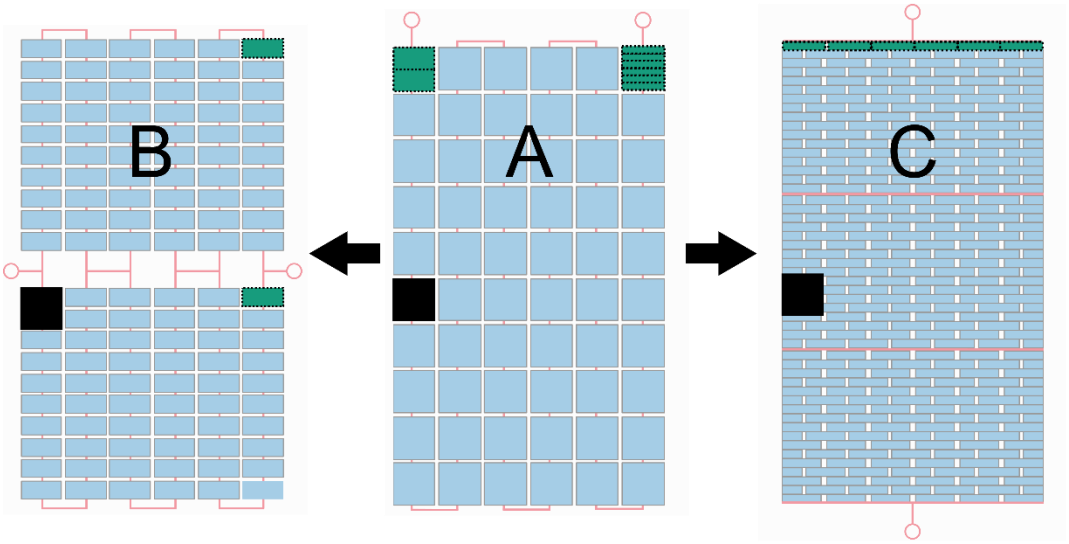

Figure 8: Principle of Distributed Current Generation in a PV Module. In scenario A, which represents the traditional design, a PV module consists of 60 square solar cells connected in series. The current for the module is generated uniformly in each solar cell, so if any cell is covered, the current for the entire string drops to zero. In scenario B, the current state-of-the-art design uses half-cut solar cells. Here, each pair of half-cells in the upper and lower parts of the module together produce the same amount of current as in scenario A. Scenario C features shingled solar cells, where six cells together generate the same current as the full square solar cells in scenario A. Unlike in scenario A, where the current-generating structures are centralized, the designs in scenarios B and C distribute these structures across the module. This distribution makes it impossible for the smallest shading structure, equivalent in size to a full square solar cell, to completely cover the current-generating areas. Larger or unusually shaped shading structures, such as a long thin line in scenario C, are needed to have the same effect. Figure reproduced from Klasen (2023).

2.4.2 Lateral current flows

Figure 9 depicts the network of resistors connecting the shingle solar cells in both the shingle string and the shingle matrix layouts. There are three types of resistors, each differing by the conductive structures in the joint (front and rear side electrode, ECA) spanning half of the shingle solar cell width. In the shingle string layout, this network extends across the entire surface of the module, while it is intermittent between the strings in the shingle string layout. Two outcomes result from this:

- All solar cells within one row are interconnected in parallel in the shingle matrix layout.
- The resistor network allows currents to flow all the way from the left to the right of the module, utilizing the conductive structures in the joint.

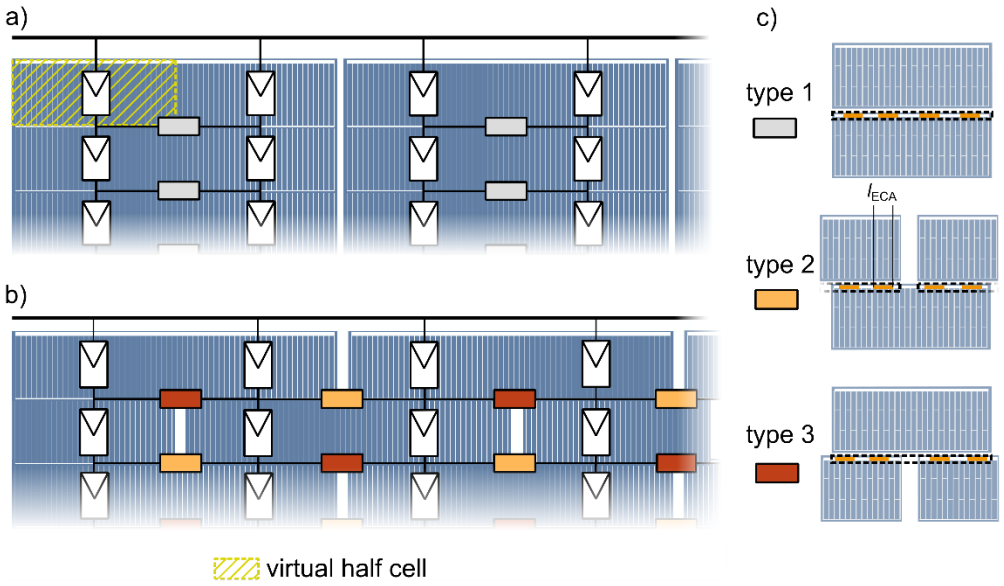

Figure 9: Shingle string (a) vs. shingle matrix layout (b). By considering a shingle solar cell to be comprised of two virtual half cells (parallel interconnected by its metallization grid), a network of resistors (types 1 to 3 as specified in (c)) can be identified, representing the conductivity in the joint perpendicular to the current flow during nominal operation. In the case of the shingle matrix, this network extends across the entire surface, allowing current paths from the right to the left side of the module using the conductive structures (electrode + ECA) in the joint. Thus, the shingle matrix layout provides improved current distribution compared to the shingle string layout. This figure is reproduced from Klasen et al. (2022a).

Since the solar cells within one row are interconnected in parallel, current mismatch between entire rows now becomes the relevant parameter for partial shading power loss. For example, in the case of diagonal shading of the module, currents can bypass the shaded area in a shingle matrix layout, while they are blocked in the shingle string layout. Instead of ceasing production, the shingle matrix module still produces significant amounts of energy in such scenarios.
More detailed explanations of this property can be found in (Klasen et al., 2022a). These lateral current flows, predicted in previous simulations, have been measured and visualized by magnetic field imaging (Klasen et al., 2023).

2.4.3 Fill Factor Effect

This property of the shingle matrix layout is rarely relevant, as it is most effective for very small shaded areas. Just as shaded solar cells in a string negatively impact their series-interconnected neighbours, the fill factor effect has a positive impact. This is evident in an increased operating voltage in rows of solar cells with higher current generation than the partially shaded row. Due to the relatively minor effect, additional details and explanations are deferred to (Klasen et al., 2022a).

2.5 Definition and Quantification

So far, we have discussed the differences in module layouts and their effects on power output under partial shading. However, to make a more fact-based comparison, we need a quantifiable measure for partial shading resilience. Previous studies have considered the average power output under partial shading (Ziar et al., 2017). While Ziar et al. (2017) used the global average power output, considering an "infinite" number of scenarios for the irradiation on each solar cell, we proposed a Monte Carlo Method (Klasen et al., 2002b) to approximate this global average by computing only a fraction of the possible combinations. Figure 10 illustrates this as the "Monte Carlo – cell level" case, which includes all possible shading scenarios as shown in (c).

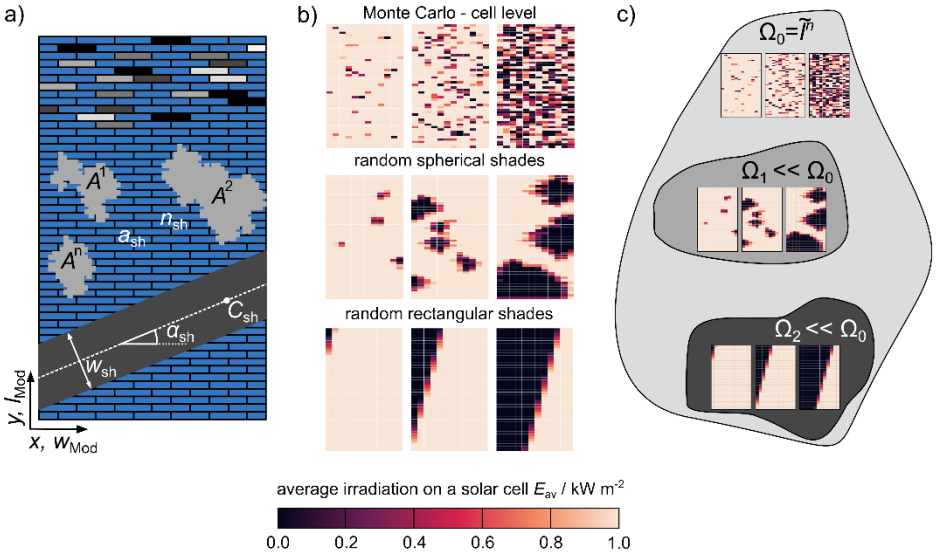

Figure 10: Monte Carlo approach for approximating the average power output of solar modules under partial shading. (a) Sketch of the three base scenarios and their parameters. (b) Three exemplary irradiation distributions for each case. (c) Visualization of the sets represented by the three approaches. Figure reproduced from Klasen et al. (2021).

These scenarios are not very representative of typical shading situations in PV systems. However, in specific cases, these random pixels form geometric shapes, which are included in subsets Ω_1 and Ω_2. These sets are still extremely large and difficult to quantify exactly. By randomizing the input values for the parameters governing the geometric shapes in these sets—hence, applying the Monte Carlo Method—we can obtain information on the average power output within these subsets. By normalizing this with the rated module power output, we get a universally comparable metric for comparing the responses of different module layouts to partial shading.

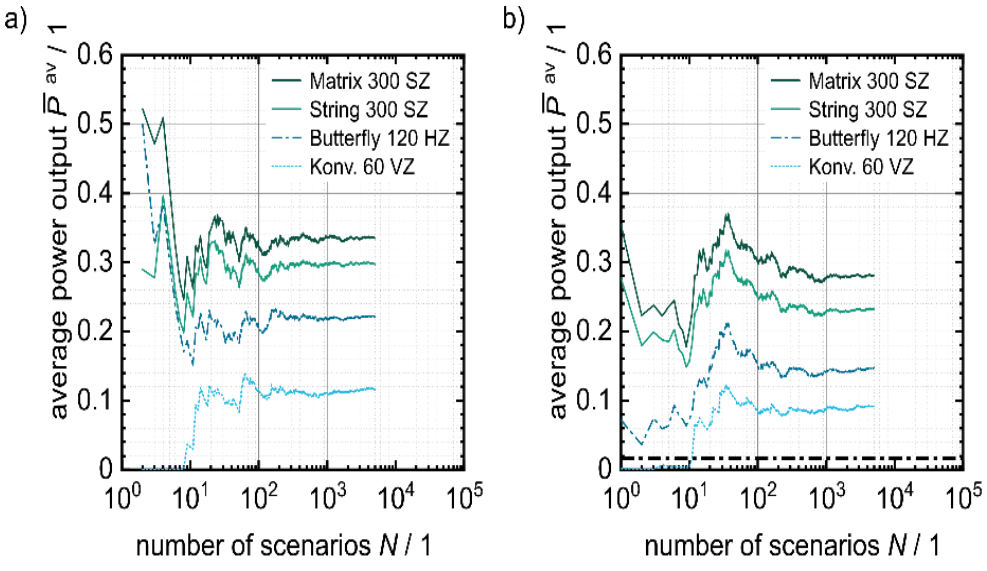

Figure 11: Results of Monte Carlo-based computation of shading resilience for (a) random rectangular and (b) random spherical shades. This study compares a conventional layout with 60 full cells, a state-of-the-art 120 half-cell butterfly layout, and two shingle layouts (string and matrix). The graphs show the evolution of average power output as the number of random computations increases, clearly demonstrating that the average values stabilize after a few thousand computations. Figure reproduced from Klasen (2023).

The results of these computations for the cases of “random spherical shades” and “random rectangular shades” are shown in Figure 11. Due to the limited relevance of a cell-based Monte Carlo scenario, those results are not included here.
After the stabilization of the normalized average power value for each layout, it becomes evident that the shingle matrix layout achieves the highest value for shading resilience in both cases. Compared to a conventional 120-cell half-cut module, the shingle matrix achieves approximately twice the output power. However, this does not mean that the shingle matrix layout will always generate the highest energy yield in installations prone to partial shading. Nonetheless, this general approach provides insights into the likely outcomes for most cases of rectangular and spherical shading.

3 Shingle Matrix Prototype Line in Freiburg, Germany

Fraunhofer ISE has established its new Module Technology Evaluation Center (Module-TEC) in Freiburg, Germany. This center features a matrix shingling pilot line for integrated photovoltaic products. The pilot line is designed to enable customers to manufacture modules at a pilot production stage (1 – 4000 pieces), suitable for certification tests or specialized showcase projects. The matrix shingle technology process sequence is illustrated in Figure 12[4]. In Figure 2, the process steps labeled “solar cell connection,” “string layup,” and “bussing” are replaced with this sequence, highlighted in blue in Figure 12.

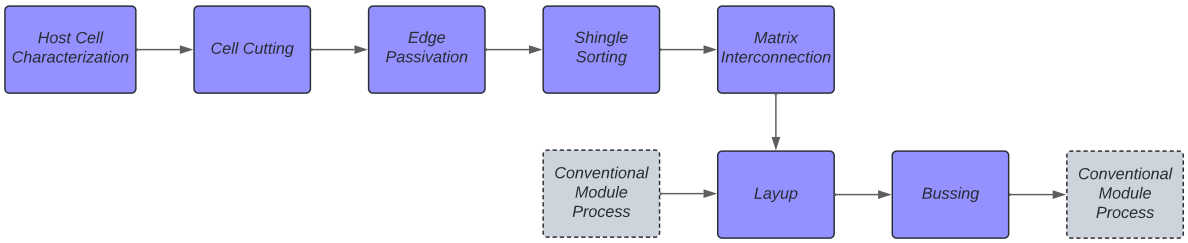

Figure 12: Matrix Shingle Technology Process Flow: The processes labeled “solar cell connection,” “string layup,” and “bussing” in Figure 2 are replaced with the steps highlighted in blue in this figure.

The pilot line begins with low-damage laser cutting to separate shingles from the host wafers. After cutting, an edge passivation layer is applied to the shingle solar cells, followed by an annealing process in the same tool. The shingles are then characterized and sorted according to their electrical output, ideally in a highly parallelized and contact-free manner. An automated guided vehicle (AGV) transports the sorted shingles to the matrix shingle stringer.

The matrix shingle stringer interconnects the shingles into the typical brickwall pattern using ECAs. The matrix is then positioned on the prepared glass and encapsulant foil during the layup step. Following this, the current must be collected from the matrix, and wiring needs to be implemented on the rear of the matrix for junction box attachment. This process, known as "bussing," uses electrically conductive tape for current collection (von Kutzleben et al., 2024).

After this overview of the matrix shingle pilot line, the process steps are described in more detail in the following sections.

3.1 Host Cell Characterization

Characterization of host cells is typically performed through current-voltage (IV) testing before shingle separation in industrial manufacturing settings. This process, essential for determining the electrical performance of the cells, is complemented by electroluminescence (EL) imaging to assess the integrity and uniformity of the cells. Based on these measurements, the host cells are sorted into different quality or BIN classes. However, this procedure does not allow for assigning individual quality classes to the individual shingles. It would be beneficial in terms of yield and performance of the module if individual shingles with defects or significant performance differences could be identified and sorted separately, as shown in Figure 13.

[4] Currently, the processes involved in the solar cell backend—specifically, cell characterization, cell cutting, edge passivation, and shingle sorting—are not co-located with the equipment used for module production.

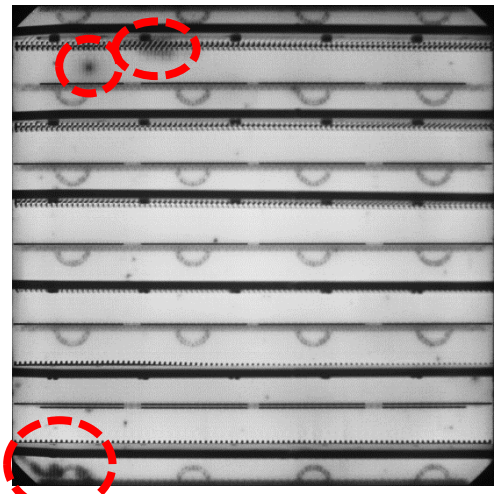

Figure 13: Electroluminescence image of an M6-sized host cell with six shingles. Each shingle is contacted with one contact bar on the front and rear sides. Visible are local defects in the uppermost and lowermost shingles (highlighted by red circles), while no significant defects are observed in the other shingles.

One approach to solving this issue is the use of predictive models based on artificial intelligence (AI) for the efficiency of shingle cells, as documented by Kunze et al. (2023). Such models are being developed within the SPHINX project to forecast post-separation performance based on local cell performance information from host cell EL images.

3.2 Shingle Separation

Fraunhofer ISE has been actively researching the properties and performance of shingled cells, as well as optimizing the cutting process, for several years (Wöhrle et al., 2017; Baliozian et al., 2018; Baliozian et al., 2021; Lohmüller et al., 2023a; Lohmüller et al., 2023b). Currently, two main shingle cutting routes are available: laser scribe and mechanical cleaving (LSMC) and thermal laser separation (TLS).

In the LSMC process, host wafers are scribed via laser ablation to a depth of several tens of microns along the desired dicing coordinates. This scribe determines the breaking points for mechanical cleaving into sub-cells (Baliozian et al., 2018). TLS, on the other hand, uses thermally induced mechanical stress for separation (Lewke, 2018; 3D-Micromac AG, 2024). Here, laser scribing is performed over a short length of a few hundred micrometers to define the starting and optional ending coordinates of the dicing street. A cleaving laser then heats the wafer along the dicing street, followed by rapid cooling using a water-air aerosol. The interaction of local heating and cooling, combined with the thermal gradient towards the chuck, leads to crack propagation in the defined direction, independent of the crystal orientation. Optimizing the TLS process for a specific wafer type requires exploring a complex, multi-dimensional parameter space (Baliozian et al., 2021).

Additionally, the laser direct cleaving (LDC) process, expected to be available at Fraunhofer ISE by mid-2024, operates on a similar principle of thermal gradient and mechanical stress as TLS but does not require water-air aerosol cooling. LDC induces a precisely defined microcrack at the cell edge, which is then guided along a nearly freely definable line to the opposite edge using the local heat of the laser. This scanner-based process allows for high travel speeds on the workpiece (Böhme and Weber, 2016; Schäfer, 2021).

Comparing LSMC with TLS and LDC reveals three main differences (Baliozian et al., 2021; Lohmüller et al., 2023a; Lewke, 2018; Schäfer, 2021). The drop in cell efficiency due to increased edge surface recombination after cutting is less pronounced with TLS. Both TLS and LDC produce smooth edges

without the damage from displaced re-solidified silicon seen in LSMC. From a factory planning perspective, the required automation concepts differ. In LSMC, host wafers remain unseparated after scribing and can be stored with standard carrier automation until the cleaving step, which can be manual or automated. In contrast, TLS and LDC fully separate the cells during the process, typically requiring pick-and-place systems to sort the shingles into carriers. Additionally, LSMC creates more debris, proportional to the scribe length, necessitating exhaust systems to ensure safety and avoid contamination.

After shingling, sub-cells can be assembled into modules. However, edge passivation is highly recommended to significantly reduce cutting-induced losses, regardless of the cutting technology used.

Finally, the (passivated) shingles can be transferred to the interconnection site, where automated guided vehicles (AGVs) can be beneficial and timesaving.

3.3 Passivated Edge Technology

Surface recombination in solar cells, which reduces the number of excited charge carriers and leads to power loss, is especially problematic at newly cut edges of solar cells that have not been passivated. This issue becomes more significant as the size of the sub-cells decreases because the ratio of edge length to surface area increases (Hermle et al., 2003; Wöhrle et al., 2017). Smaller cells, like shingle cells, are more affected by edge recombination, especially when they have higher efficiency potential. While edge recombination also affects today's half or third cells, it is particularly critical for shingle cells.

Thus, for fabrication of highly efficient shingle cells/modules, edge recombination must be decreased. First, the cutting of the cells should be performed with low damage technologies, such as TLS or LDC, as has been described in the section before. Second, the charge carrier recombination at the newly created edge surfaces needs to be minimized. This can be achieved by, for example, edge passivation (Zhao et al., 2000; Hermle et al., 2003; Guo et al., 2007). Fraunhofer ISE filed patent applications for edge passivation in 2018 after very encouraging proof-of-concepts and modelling of the respective improvement potentials (Wöhrle et al., 2017). In 2019, Fraunhofer ISE introduced the post-metallization passivated edge technology (PET) and demonstrated back then edge passivation on bifacial PERC shingle solar cells (Baliozian et al., 2019; Baliozian et al., 2020). The PET is a proprietary development of Fraunhofer ISE to address the cutting losses in today’s solar cells by a simple, high-throughput post-processing on separated solar cells. It consists of the deposition of a dielectric passivation layer after cell separation, for example, an aluminium oxide (Al_2O_3) layer which is well known for its excellent surface passivation quality (Richter et al., 2011), and an optional subsequent annealing step for Al_2O_3 layer activation. During fabrication of TOPCon solar cells, similar high-temperature processing is applied as for PERC, making their production compatible with existing mass fabrication as well as with PET treatment without additional temperature range restrictions. On the other hand, the process temperatures for amorphous silicon-based heterojunction (SHJ) cells needs to be kept below around 200 °C (Haschke et al., 2019; Luderer et al., 2020). As the Al_2O_3 deposition is performed as a low-temperature process with temperatures below 200 °C, special caution is only necessary for the annealing step in SHJ cells. Besides PERC, as mentioned above, the PET has also been demonstrated by Fraunhofer ISE on TOPCon shingle cells (Lohmüller et al., 2023a; 2023b) as well as on SHJ half-cells (Münzer et al., 2021). The concept of the PET approach was taken up by CEA-INES in 2020

(Harrison et al., 2020) and demonstrated on SHJ shingle cells (Harrison et al., 2020; Portaluppi et al., 2020; Harrison et al., 2022; Martel et al., 2023).

Initially, the PET approach with Al_2O_3 passivation layer has been applied at Fraunhofer ISE using a lab-scale thermal atomic layer deposition (T-ALD) tool, the "FlexAl" system from *Oxford Instruments*. During Al_2O_3 deposition, the shingle solar cells are stacked closely on top of each other. Nowadays, a high-throughput plasma-enhanced ALD (PE-ALD) prototype tool, the "LINEA" system from *Plasma Electronic* is used for edge passivation with Al_2O_3. The singulated solar cells can be stacked in quite large quantities. Assuming a cell thickness of 200 µm (including metallization) and a cell stack height of 9 cm, 450 cells can be stacked on top of each other. With a gap of 1 cm between the cell stacks in x- and y-direction, 54,000 shingle solar cells can be processed per run for a M10 1/6 cell format; see Table 1. This is equivalent to 9,000 full-format host cells. Excluding wafer and tray handling, one PE-ALD run currently takes about 1 h. In terms of solar cell production capability, this corresponds to a throughput of about 0.6 GW_p per year for this PE-ALD process. Through further hardware and process optimizations, process times of around 15 min per PE-ALD run can become quite realistic in the near future. This would lead to an increase of the solar cell production capability of the PE-ALD prototype tool to about 2.5 GW_p per year for M10 1/6 shingle cells.

Table 1: Estimation of the number of cells with various geometries that can be processed in a single PE-ALD run, with durations of either 1 hour or 15 minutes, in a chamber with a volume of approximately 1×1×0.1 m³. The cell thickness, including metallization, is considered to be 200 µm. Each stack, with a height of 9 cm, consists of 450 cells. The gap between the cell stacks on each side is assumed to be 1 cm.

Wafer format	**Edge length host cell (mm)**	**Number 1/6th shingle cells per hour**		**Number half cells per hour**	
Run duration PE-ALD ->		**1 h**	**15 min**	**1 h**	**15 min**
G1	158.75	60,750	243,000	24,750	99,000
M6	166	58,500	234,000	22,500	90,000
M10	182	54,000	216,000	20,250	81,000
G12	210	39,600	158,400	14,400	57,600

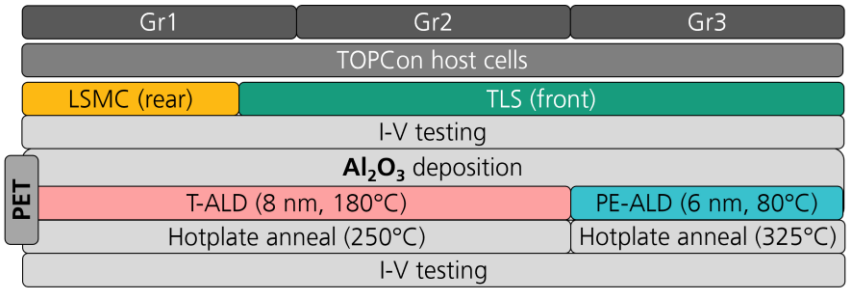

Figure 14: Schematic of the process sequence used for examining cell separation and edge passivation for TOPCon shingle solar cells. The host cells are tested monofacially for their current-voltage (IV) data on black foil using GridTouch with 30 wires per side (perpendicular to the busbars). The shingle cells are also tested monofacially (no rear side illumination), using pin contact strips. The graph is adapted from Lohmüller et al.(2023a).

Figure 14 presents the schematic of an experiment (Lohmüller et al., 2023a) comparing LSMC and TLS for separating G1 format host cells into six shingle cells each. For PET, the T-ALD and PE-ALD approaches are evaluated against each other. The annealing step is conducted on a hotplate at 250°C for T-ALD (Gr1 and Gr2) and 325°C for PE-ALD (Gr3), each for 25 minutes.

The results are illustrated in Figure 15. First, the TLS cutting in Gr2 and Gr3 shows an efficiency advantage of $\Delta\eta$ = 0.2%$_{abs}$ compared to the LSMC cutting in Gr1. Second, application of the PET leads to an efficiency improvement of $\Delta\eta$ = 0.4%$_{abs}$ for the T-ALD route in Gr1 and Gr2, no matter which separation technology is applied. Third, PET via the PE-ALD route leads to $\Delta\eta$ = 0.5%$_{abs}$ for Gr3 after edge passivation. With respect to the reference group Gr1, whose shingle cells have been separated by LSMC and did not receive edge passivation, the combination of TLS and PE-ALD Al_2O_3 results in TOPCon shingle cells with a mean efficiency advantage of +0.7%$_{abs}$. This corresponds to an efficiency recovery of up to about 80%. This is a remarkable demonstration of the benefit provided by PET with high-throughput ALD of Al_2O_3 in conjunction with low-damage cell cutting. Apart from hotplate annealing, Fraunhofer ISE lately also successfully tested several high throughputs annealing process possibilities.

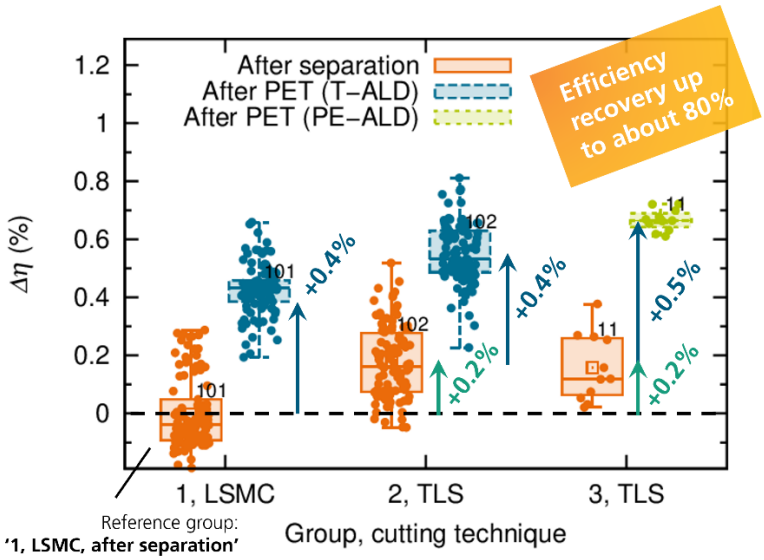

Figure 15: IV data for the three TOPCon solar cell groups, expressed as an absolute offset from the mean of the respective reference group stated. The graph is adapted from Lohmüller et al. (2023a).

3.4 Shingle Characterization

Following the separation process and edge passivation step, shingle cells undergo a series of quality and process control measures. Within the SPHINX project, we prioritize techniques such as photoluminescence imaging and optical inspection to ensure the high quality of shingle cells. Additionally, conventional IV characterization is applied as a reference. Shingles are sorted into specific quality classes to prevent mismatch losses during their serial interconnection. Due to the multiplication of samples by a factor of six to eight compared to the host cell, the throughput of shingle cell characterization becomes critical. To manage this efficiently, we aim to employ high-throughput techniques, including the parallel characterization of multiple shingle cells.

To streamline this procedure, SPHINX is conducting extensive testing on large quantities of shingle solar cells to determine whether post-passivation classification is necessary or if a host cell, AI-based prediction algorithm could suffice. This involves experimenting with a statistically significant number

of solar cells to identify the optimal location for *IV* measurement and developing an AI algorithm that can accurately predict individual shingle *IV* characteristics.

Another approach is to use photoluminescence imaging on shingle cells as an addition to *IV* characterization of host cells, which can also be performed simultaneously on multiple shingle cells. This method allows us to control the cutting and edge passivation processes and to identify and exclude defective cells at this stage.

Shingle cell characterization is a cornerstone of the SPHINX project, laying the groundwork for shingle matrix technology that promises to revolutionize the integration of photovoltaics in various applications. The meticulous analysis and subsequent improvements in shingle cell design and function are expected to lead to enhanced module efficiencies and robust, resilient energy-generating technology suitable for urban landscapes.

3.5 Matrix Interconnection

Once the shingles are cut, passivated, and sorted, they are connected with ECA in a brick wall pattern using the matrix shingle stringer. The prototype matrix shingle stringer used in the pilot line was developed by M10 Industries as part of the "Shirkan" project, substantially funded by the BMWi in Germany. Figure 16 depicts the prototype stringer and its components for processing shingles into matrices. The machine has a theoretical throughput of 2,800 shingles per hour.

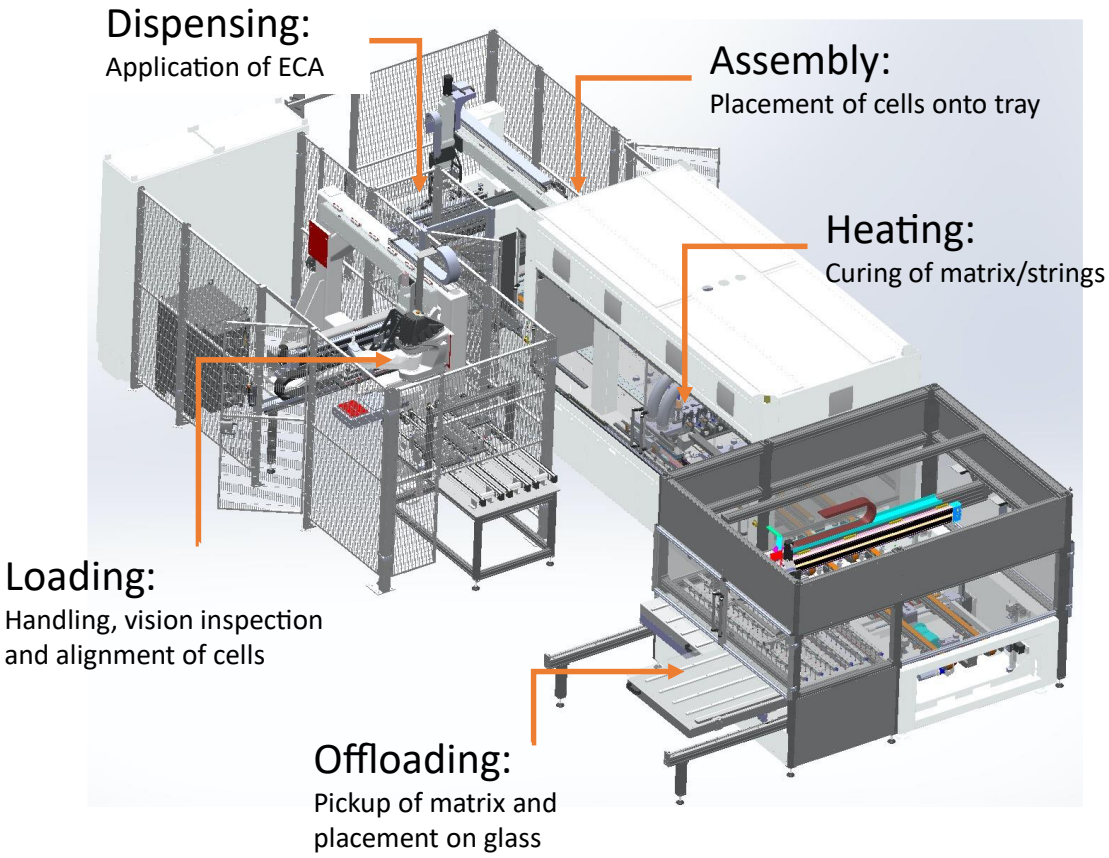

Figure 16: Prototype matrix shingle stringer with the capability to produce at a throughput of 2800 shingles per hour.

3.6 Bussing and Diode Integration

The current generated by the assembled shingle matrix must be efficiently collected and transferred to the module's junction boxes. Traditional soldering of a bus connector across the entire matrix width is impractical due to the mismatch in the coefficient of thermal expansion between the copper-based bussing ribbons and the silicon of the shingled solar cells. This mismatch induces significant thermomechanical stress, causing warping of the solar cell matrix.

To address this issue, shingled matrix technology employs electrically conductive tapes that do not require additional curing (von Kutzleben et al., 2024). These tapes consist of a copper foil substrate with a layer of pressure-sensitive adhesive containing dispersed electrically conductive particles. The particles create an electrical connection between the shingle matrix and the copper substrate through mechanical interlocking.

While the contact resistance of the tape is relatively high, it effectively covers a large area. The end cells of the matrix visually cover the tape, which is placed on the backside of these cells, including for front contact. However, these covering cells are bypassed and do not contribute to electricity generation. These tapes facilitate easy and cost-efficient automation and can be attached at several positions in the matrix. This flexibility allows for the addition of more bypass diodes if enhanced hotspot protection is needed.

The ribbons leading to the junction boxes are connected to the conductive tapes and laid behind the solar cell matrix.

3.7 Module Lamination, Framing and J-Box and I-V Characterization of Modules

After the fabrication of the matrix in the stringer and the application of electrically conductive tapes and bussing ribbons, another layer of encapsulant foil and the backsheet are positioned on the laminate. The entire stack is inspected for defects using electroluminescence (EL) imaging before it is fed into the flat-plate lamination process Figure 17. The lamination process requires only minor adjustments, as this and the subsequent processes are essentially the same as those used in conventional module production.

The junction box, attached to the rear of the PV module, is crucial for electrical connections and houses bypass diodes that prevent hotspots caused by shading or cell damage. Meanwhile, the anodized aluminum frame enhances structural integrity, aiding in installation and providing resistance to environmental stresses like wind and snow. It also grounds the module, reducing electrical hazards.

Figure 17: Photovoltaic module laminator capable of performing plate-membrane, plate-plate laminations as well as cooling arranged in stacks.

3.8 Reliability

To evaluate the stability and electrical safety of shingle matrix modules various environmental stress scenarios were applied (Abdel Latif et al., 2023). Accelerated aging tests and sequences as defined in IEC 61215-2:2021 and IEC 61730-2:2016 were conducted in accordance with IEC 17025 certification procedures at the Fraunhofer ISE's PV Modules TestLab. Table 2 shows the number of tested modules and the corresponding relative power loss after the tests or sequence.

Table 2: Tests and sequences with the corresponding average degradation in the maximum power point.

Test / Sequence	Standard	No. of Modules	Relative power degradation / %
Hot-spot endurance test	IEC 61215	1	−0.3 %
TC200	IEC 61215	4	−0.58 %
DH1000 + ML	IEC 61215	3	−2.10 % / −2.46 %
TC50 + HF10	IEC 61215	1	−0.66 % / −3.26 %
Material creep test	IEC 61730	1	/
Sequence B1	IEC 61730	1	−7.5 %

All the standard's requirements for maximum power loss and electrical safety across all test scenarios were met. Performance degradation after thermal cycling (TC) and mechanical load (ML) tests was better than historical median values from module certification data, as shown in Figure 18 (Gebhardt et al., 2021). However, in the damp heat (DH) test, the modules performed slightly worse. Minor irregularities observed in Electroluminescence (EL) images are attributed to production inaccuracies and are expected to be easily rectifiable in future productions. No visual defects or deterioration in electrical insulation were detected. A maximum temperature of around 104 °C in the hot spot test

indicates a low risk of hot spot formation under partial shading. The results of the material creep test and sequence B1, as per IEC 61730, revealed no significant electrical safety issues, even under combined environmental stress. These findings demonstrate the high potential and readiness of shingle matrix modules for commercialization with respect to certification. It is anticipated that modules produced from an optimized industrial line will show even better reliability due to the ease of resolving minor material and handling issues.

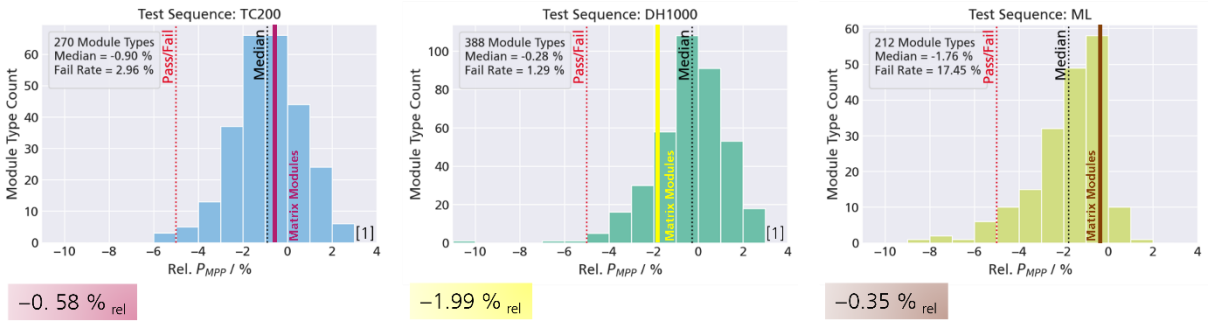

Figure 18: Test results of shingle matrix modules in comparison to historical module data. Shingle matrix modules perform better in TC and ML tests. DH reveals potential to improve the encapsulation of the modules.

4 Conclusion and Recommendation

The matrix shingle technology presents a significant advancement in photovoltaic module design, addressing several key challenges faced by conventional PV modules. By cutting full wafer solar cells into narrow cell stripes and interconnecting them in a brick wall pattern using ECAs, this technology maximizes the active photovoltaic area within the module. This design not only eliminates the need for interconnector wires but also enhances the aesthetic appeal of the modules, making them particularly suitable for applications in building-integrated photovoltaics (BIPV) and other integrated PV solutions.

One of the primary advantages of matrix shingle technology is its adaptability to various environments and applications. In BIPV, for instance, the ability to customize the size and shape of the modules allows for seamless integration into building facades and roofs, improving both energy efficiency and architectural aesthetics. Similarly, in vehicle-integrated photovoltaics (VIPV) and agrivoltaics (AV), the flexible design of the shingle modules enables optimal energy generation without compromising the functionality or appearance of the host structures.

The technological advancements incorporated in matrix shingle technology, such as TLS and edge passivation, significantly enhance the efficiency and reliability of the modules. TLS ensures smoother cuts and less damage, resulting in higher cell efficiency, while edge passivation reduces recombination losses at the cell edges. Additionally, the use of electrically conductive tapes for current collection and the strategic placement of bypass diodes further improves the durability and performance of these modules, especially under partial shading conditions.

Looking forward, the continued development and optimization of matrix shingle technology hold great promise for the future of integrated photovoltaics. As the technology matures, it is expected to drive further growth and adoption in the IPV market, offering a versatile and efficient solution for sustainable energy generation. The potential for high-throughput production, coupled with ongoing innovations, positions matrix shingle technology as a key player in the transition towards a more sustainable and renewable energy future.

5 Risks and Interconnections

Several risks could impact the success of the matrix shingling pilot line. Technological risks include efficiency in edge passivation and throughput in TLS processes. Production risks involve scaling issues and automation shortcomings. Market risks encompass slow adoption and cost competitiveness. Environmental and regulatory risks pertain to long-term durability and compliance challenges. Supply chain risks highlight potential material shortages and logistics issues. Operational risks include maintenance needs and skill shortages. Mitigation strategies focus on optimizing processes, ensuring quality, educating the market, diversifying suppliers, and investing in training and maintenance.

Risk No.	What is the risk	Probability of risk occurrence[1]	Effect of risk[1]	Solutions to overcome the risk
1	Limited efficiency gains from edge passivation quality	2	1	Enhance the edge passivation process
2	Throughput and availability issues with the TLS process	1	1	Utilize alternative cutting processes and invest in high-throughput equipment
3	Production scaling challenges	2	2	Simplify production methods, gradually increase volumes, and collaborate with industrial partners for scaling expertise.
4	Inability to fully automate processes	1	2	Prioritize high-impact quality or throughput processes. Implement semi-automatic solutions to maintain reasonable throughput.
5	Slow market adoption	2	2	Enhance marketing efforts and provide education on the benefits of matrix shingle technology. Engage with stakeholders and potential customers early.
6	Cost competitiveness	2	2	Optimize production processes to reduce costs. Explore alternative materials and suppliers to lower expenses.
7	Module reliable and compliance to regulations	3	2	Conduct thorough reliability testing and ensure compliance with all relevant regulations. Adapt module designs and BOM to enhance durability.
8	Sourcing issues of high quality shingle cells	2	1	Diversify suppliers, maintain buffer stocks of critical materials, and consider

				reverting to “H-pattern shingling”.
9	Personnel shortages	3	1	Invest in efficient staff training programs and partner with educational institutions for workforce development.

[1)] Probability risk will occur: 1 = high, 2 = medium, 3 = Low

6 References

3D-Micromac AG. (2024). *MicroDICE - Laser Wafer Dicing System for SiC, GaN, and Silicon* [Company Website]. https://3d-micromac.de/laser-mikrobearbeitung/produkte/microdice/

Abdel Latif, N., Markert, J., von Kutzleben, D., Birnkammer, S., Rößler, T., Weber, J., Kraft, A., & Neuhaus, H. (2023). Design, Manufacturing and Reliability of Shingle Matrix Modules. *Proceedings of the 40th European Photovoltaic Solar Energy Conference & Exhibition*, 020261-001-020261–006. https://doi.org/10.4229/EUPVSEC2023/3DO.18.1

Allsopp, B. L., Orman, R., Johnson, S. R., Baistow, I., Sanderson, G., Sundberg, P., Stålhandske, C., Grund, L., Andersson, A., Booth, J., Bingham, P. A., & Karlsson, S. (2020). Towards improved cover glasses for photovoltaic devices. *Progress in Photovoltaics: Research and Applications*, *28*(11), 1187–1206. https://doi.org/10.1002/pip.3334

Baliozian, P., Al-Akash, M., Lohmüller, E., Richter, A., Fellmeth, T., Münzer, A., Wöhrle, N., Saint-Cast, P., Stolzenburg, H., Spribille, A., & Preu, R. (2020). Postmetallization "Passivated Edge Technology" for Separated Silicon Solar Cells. *IEEE Journal of Photovoltaics*, *10*(2), 390–397. https://doi.org/10.1109/JPHOTOV.2019.2959946

Baliozian, P., Klasen, N., Wöhrle, N., Kutter, C., Stolzenburg, H., Münzer, A., Saint-Cast, P., Mittag, M., Lohmüller, E., Fellmeth, T., Al-Akash, M., Kraft, A., Heinrich, M., Richter, A., Fell, A., Spribille, A., Neuhaus, H. D., & Preu, R. (2019). PERC-based shingled solar cells and modules at Fraunhofer ISE. *Photovoltaics International*, *43*, 129–145.

Baliozian, P., Lohmüller, E., Fellmeth, T., Wöhrle, N., Krieg, A., & Preu, R. (2018a). Bifacial p-Type Silicon Shingle Solar Cells – the "pSPEER" Concept. *Solar RRL*, *2*(3), 1700171. https://doi.org/10.1002/solr.201700171

Baliozian, P., Lohmüller, E., Fellmeth, T., Wöhrle, N., Krieg, A., & Preu, R. (2018b). *Bifacial shingle solar cells on p-type Cz-Si (pSPEER)*. 110002. https://doi.org/10.1063/1.5049311

Baliozian, P., Münzer, A., Lohmüller, E., Nair, A., Fellmeth, T., Wöhrle, N., Höffler, H., Spribille, A., & Preu, R. (2021). Thermal Laser Separation of PERC and SHJ Solar Cells. *IEEE Journal of Photovoltaics*, *11*(2), 259–267. https://doi.org/10.1109/JPHOTOV.2020.3041251

Böhme, R., & Weber, D. (2016). *Verfahren und Vorrichtung zum laserbasierten Bearbeiten von flächigen, kristallinen Substraten, insbesondere von Halbleitersubstraten* (Patent No. WO2016008768A1).

C. Dickson Jr., D. (1960). *Photo-voltaic semiconductor apparatus or the like* (Patent No. US2938938A).

Dullweber, T., & Tous, L. (2021). *Silicon Solar Cell Metallization and Module Technology*. The Institution of Engineering and Technology (IET).

Gebhardt, P., Mülhöfer, G., Roth, A., & Philipp, D. (2021). Statistical analysis of 12 years of standardized accelerated aging in photovoltaic-module certification tests. *Progress in Photovoltaics: Research and Applications*, *29*(12), 1252–1261. https://doi.org/10.1002/pip.3450

Geipel, T. (2017). *Electrically conductive adhesives for photovoltaic modules*. Fraunhofer Verlag. https://publica.fraunhofer.de/handle/publica/282389

Green, M. A. (2015). The Passivated Emitter and Rear Cell (PERC): From conception to mass production. *Solar Energy Materials and Solar Cells*, *143*, 190–197. https://doi.org/10.1016/j.solmat.2015.06.055

Guo, J.-H., Cotter, J., McIntosh, K., Fisher, K., Chen, F., & Karpour, A. (2007). Edge passivation for small-area, high efficiency solar cells. *Proceedings of the 22nd European Photovoltaic Solar Energy Conference and Exhibition*, 1348–1351.

Harrison, S., Barth, V., Carrière, C., Albaric, M., Martel, B., Galiazzo, M., Sovernigo, E., & Frasson, N. (2022). Simplified Cell Cutting, Efficient Edge Passivation, Copper Metallization: Tackling the last Hurdles for Optimized SHJ Integration in Shingle Module Configuration. *Proceedings of the 8th World Conference on Photovoltaic Energy Conversion*, 55–58. https://doi.org/10.4229/WCPEC-82022-1BO.2.1

Harrison, S., Bettinelli, A., Portaluppi, B., Giglia, V., Carrière, C., Sekkat, A., Munoz-Rojas, D., & Barth, V. (2020). Challenges for Efficient Integration of SHJ Based Solar Cells in Shingle Module Configuration. *Proceedings of the 37th European Photovoltaic Solar Energy Conference and Exhibition*, 223–227. https://doi.org/10.4229/EUPVSEC20202020-2BO.5.5

Haschke, J., Lemerle, R., Aissa, B., Abdallah, A. A., Kivambe, M. M., Boccard, M., & Ballif, C. (2019). Annealing of Silicon Heterojunction Solar Cells: Interplay of Solar Cell and Indium Tin Oxide Properties. *IEEE Journal of Photovoltaics*, *9*(5), 1202–1207. https://doi.org/10.1109/JPHOTOV.2019.2924389

Hermle, M., Dicker, J., Warta, W., Glunz, S., & Willeke, G. (2003). Analysis of edge recombination for high-efficiency solar cells at low illumination densities. *Proceedings of 3rd World Conference on Photovoltaic Energy Conversion*, 1009–1012.

Huyeng, J. D., Lohmüller, E., Rößler, T., Shabanzadeh, B., Reichel, C., Weber, J., Hofmann, M., von Kutzleben, D., Abdel Latif, N., Kraft, A., Neuhaus, H., Clement, F., & Preu, R. (2023). Challenges and Advantages for Cut Solar Cells for Shingling and Half-Cell Modules. *Proceedings of the 40th European Photovoltaic Solar Energy Conference & Exhibition*, 020039-001-020039–005. https://doi.org/10.4229/EUPVSEC2023/1BV.5.42

IMARC. (2023). *Building Integrated Photovoltaics Market Report by Product Type (Polycrystalline, Thin Film, and Others), Application (Roof, Facades, Glass, and Others), End Use (Commercial, Residential, Industrial), and Region 2024-2032* (No. SR112024A2098). https://www.imarcgroup.com/building-integrated-photovoltaics-market

IRENA. (2023). *Renewable power generation costs in 2022*. https://www.irena.org/Publications/2023/Aug/Renewable-Power-Generation-Costs-in-2022

Jelle, B. P. (2016). Building Integrated Photovoltaics: A Concise Description of the Current State of the Art and Possible Research Pathways. *Energies*, *9*(1), 21. https://doi.org/10.3390/en9010021

Kavlak, G., McNerney, J., & Trancik, J. E. (2018). Evaluating the causes of cost reduction in photovoltaic modules. *Energy Policy*, *123*, 700–710. https://doi.org/10.1016/j.enpol.2018.08.015

Klasen, N. (2023). *Elektrisches und mechanisches Design von Solarmodulen mit geschindelten Solarzellen*. Fraunhofer-Verlag. https://publica.fraunhofer.de/handle/publica/456721

Klasen, N., Lux, F., Weber, J., Weißer, D., Roessler, T., Kraft, A., & Neuhaus, D. H. (2021). Quantitative Evaluation of the Shading Resilience of PV Modules. *Proceedings of the 38th European Photovoltaic Solar Energy Conference and Exhibition*, 560–567. https://doi.org/10.4229/EUPVSEC20212021-4BO.2.6

Klasen, N., Weisser, D., Rößler, T., Neuhaus, D. H., & Kraft, A. (2022a). Performance of shingled solar modules under partial shading. *Progress in Photovoltaics: Research and Applications*, *30*(4), 325–338. https://doi.org/10.1002/pip.3486

Klasen, N., Lux, F., Weber, J., Roessler, T., & Kraft, A. (2022b). A Comprehensive Study of Module Layouts for Silicon Solar Cells Under Partial Shading. *IEEE Journal of Photovoltaics*, *12*(2), 546–556. https://doi.org/10.1109/JPHOTOV.2022.3144635

Klasen, N., Weber, J., Kraft, A., & Neuhaus, H. (2023). Lateral Currents in Shingle Solar Modules Detected by Magnetic Field Imaging. *IEEE Journal of Photovoltaics*, *13*(4), 552–557. https://doi.org/10.1109/JPHOTOV.2023.3271892

Kuhn, T. E., Erban, C., Heinrich, M., Eisenlohr, J., Ensslen, F., & Neuhaus, D. H. (2021). Review of technological design options for building integrated photovoltaics (BIPV). *Energy and Buildings*, *231*, 110381. https://doi.org/10.1016/j.enbuild.2020.110381

Kunze, P., Demant, M., Krieg, A., Tummalieh, A., Wöhrle, N., & Rein, S. (2023). Shingle cell IV characterization based on spatially resolved host cell measurements. *Progress in Photovoltaics: Research and Applications*, pip.3764. https://doi.org/10.1002/pip.3764

Lewke, D. (2018). *Untersuchung und Minimierung lateraler Rissabweichungen beim Thermischen Laserstrahlseparieren*. Shaker.

Lohmüller, E., Baliozian, P., Gutmann, L., Kniffki, L., Beladiya, V., Geng, J., Wang, L., Dunbar, R., Lepert, A., Hofmann, M., Richter, A., & Huyeng, J. D. (2023). Thermal laser separation and high-throughput layer deposition for edge passivation for TOPCon shingle solar cells. *Solar Energy Materials and Solar Cells*, *258*, 112419. https://doi.org/10.1016/j.solmat.2023.112419

Lohmüller, E., Baliozian, P., Gutmann, L., Kniffki, L., Richter, A., Wang, L., Dunbar, R., Lepert, A., Huyeng, J. D., & Preu, R. (2023). TOPCon shingle solar cells: Thermal laser separation and passivated edge technology. *Progress in Photovoltaics: Research and Applications*, *31*(7), 729–737. https://doi.org/10.1002/pip.3680

Luderer, C., Messmer, C., Hermle, M., & Bivour, M. (2020). Transport Losses at the TCO/a-Si:H/c-Si Heterojunction: Influence of Different Layers and Annealing. *IEEE Journal of Photovoltaics*, *10*(4), 952–958. https://doi.org/10.1109/JPHOTOV.2020.2983989

Martel, B., Albaric, M., Harrison, S., Dhainaut, F., & Desrues, T. (2023). Addressing separation and edge passivation challenges for high efficiency shingle heterojunction solar cells. *Solar Energy Materials and Solar Cells*, *250*, 112095. https://doi.org/10.1016/j.solmat.2022.112095

Mittag, M., Pfreundt, A., & Shahid, J. (2020). Impact of Solar Cell Dimensions on Module Power, Efficiency and Cell-To-Module Losses. *Proceedings of the 30th PV Solar Energy Conference (PVSEC-30)*, 1–6. https://doi.org/10.24406/PUBLICA-FHG-410769

Mittag, M., Zech, T., Wiese, M., Blasi, D., Ebert, M., & Wirth, H. (2017). Cell-to-Module (CTM) Analysis for Photovoltaic Modules with Shingled Solar Cells. *2017 IEEE 44th Photovoltaic Specialist Conference (PVSC)*, 1531–1536. https://doi.org/10.1109/PVSC.2017.8366260

Mondon, A., Klasen, N., Fokuhl, E., Mittag, M., Heinrich, M., & Wirth, H. (2018). Comparison of Layouts for Shingled Bifacial PV Modules in Terms of Power Output, Cell-to-Module Ratio and Bifaciality. *Proceedings of the 35th European Photovoltaic Solar Energy Conference and Exhibition;*, 1006–1010. https://doi.org/10.4229/35THEUPVSEC20182018-5BO.9.3

Münzer, A., Baliozian, P., Ahmed, K., Nair, A., Lohmüller, E., Fellmeth, T., Spribille, A., & Preu, R. (2020). Laser Assisted Separation Processes for Bifacial pSPEER Shingle Solar Cells. *Proceedings of the 37th European Photovoltaic Solar Energy Conference and Exhibition*, 394–399. https://doi.org/10.4229/EUPVSEC20202020-2CV.1.51

Münzer, A., Baliozian, P., Steinmetz, A., Geipel, T., Pingel, S., Richter, A., Roder, S., Lohmüller, E., Spribille, A., & Preu, R. (2021). Post-Separation Processing for Silicon Heterojunction Half Solar Cells With Passivated Edges. *IEEE Journal of Photovoltaics*, *11*(6), 1343–1349. https://doi.org/10.1109/JPHOTOV.2021.3099732

Photovoltaic (PV) Module Safety Qualification: Part 2: Requirements for Testing (Standard No. IEC 61730-2; 2.0). (2016). International Electrotechnical Commission (IEC). https://doi.org/10.13140/RG.2.2.30892.72327

Portaluppi, B., Harrison, S., Giglia, V., Sekkat, A., & Munoz-Rojas, D. (2020). Insights on Cell Edge Defects Impact and Post-Process Repassivation for Heterojunction. *Proceedings of the 37th European Photovoltaic Solar Energy Conference and Exhibition*, 504–507. https://doi.org/10.4229/EUPVSEC20202020-2DV.3.16

Richter, A., Benick, J., Hermle, M., & Glunz, S. W. (2011). Excellent silicon surface passivation with 5 Å thin ALD Al_2O_3 layers: Influence of different thermal post-deposition treatments. *Physica Status Solidi (RRL) – Rapid Research Letters*, *5*(5–6), 202–204. https://doi.org/10.1002/pssr.201105188

Rößler, T., Von Kutzleben, D., Klasen, N., Nikitina, V., Baliozian, P., Münzer, A., Fokuhl, E., & Kraft, A. (2022). *Progress in shingle interconnection based on electrically conductive adhesives at Fraunhofer ISE*. 020012. https://doi.org/10.1063/5.0127455

Schäfer, E. (2021). And… Cut!: Innovative laser cutting technologies in photovoltaics. *PhotonicsViews*, *18*(1), 69–71. https://doi.org/10.1002/phvs.202000049

Schmidt, W., & Rasch, K.-D. (1990). New interconnection technology for enhanced module efficiency. *IEEE Transactions on Electron Devices*, *37*(2), 355–357. https://doi.org/10.1109/16.46366

Schulte-Huxel, H., Kraft, A., Roessler, T., & De Rose, A. (2021). Module interconnection technologies. In *Silicon Solar Cell Metallization and Module Technology* (pp. 435-489 (55)). The Institution of Engineering and Technology (IET).

Statista. (2023). *Annual solar module production worldwide 2000 to 2022*. https://www.statista.com/statistics/668764/annual-solar-module-manufacturing-globally/

Sunpower/Maxeon. (2024). *Performance Solar Panels*. https://maxeon.com/us/solar-panel-products/performance-solar-panels

The Business Research Company. (2023). *Building-integrated Photovoltaics Global Market Report 2024* (No. ID: 5741663; p. 200).

Tous, L., Govaert, J., Harrison, S., Carrière, C., Barth, V., Giglia, V., Buchholz, F., Chen, N., Halm, A., Faes, A., Nogay, G., Quest, H., Roessler, T., Fellmeth, T., Reinwand, D., Stolzenburg, H., Schindler, F., Mittag, M., Morlier, A., … Gordon, I. (2023). Overview of key results achieved in H2020 HighLite project helping to raise the EU PV industries' competitiveness. *Progress in Photovoltaics: Research and Applications*, *31*(12), 1409–1427. https://doi.org/10.1002/pip.3667

VDMA. (2011). *International Roadmap for Photovoltaic (ITRPV):2010 Results*.

VDMA. (2012). *International Roadmap for Photovoltaic (ITRPV):2011 Results*.

VDMA. (2013). *International Roadmap for Photovoltaic (ITRPV):2012 Results*.

VDMA. (2014). *International Roadmap for Photovoltaic (ITRPV):2013 Results*.

VDMA. (2015). *International Roadmap for Photovoltaic (ITRPV):2014 Results*.

VDMA. (2016). *International Roadmap for Photovoltaic (ITRPV):2015 Results*.

VDMA. (2017). *International Roadmap for Photovoltaic (ITRPV):2016 Results*.

VDMA. (2018). *International Roadmap for Photovoltaic (ITRPV):2017 Results*.

VDMA. (2019). *International Roadmap for Photovoltaic (ITRPV):2018 Results*.

VDMA. (2020). *International Roadmap for Photovoltaic (ITRPV):2019 Results*.

VDMA. (2021). *International Roadmap for Photovoltaic (ITRPV):2020 Results*.

VDMA. (2022). *International Roadmap for Photovoltaic (ITRPV):2021 Results*.

VDMA. (2023). *International Roadmap for Photovoltaic (ITRPV):2022 Results*.

VDMA. (2024). *International Roadmap for Photovoltaic (ITRPV):2023 Results*.

von Kutzleben, D., Rößler, T., Mittag, M., Weber, J., Sigdel, S., Klasen, N., Zahn, P., Kraft, A., & Neuhaus, H. D. (2022). Development of Shingle Matrix Technology for Integrated Applications. *Proceedings of the 8th World Conference on Photovoltaic Energy Conversion*. 8th World Conference on Photovoltaic Energy Conversion, Milano.

von Kutzleben, D., Weber, J., Abdel Latif, N., Rößler, T., Kraft, A., & Neuhaus, H. D. (2024, to be published). Reliable and Automatable Solution for Shingle Bussing. *Proceedings of the 52nd IEEE Photovoltaic Specialists Conference*. 52nd IEEE Photovoltaic Specialists Conference (52nd IEEE PCVSC), Seattle.

Wirth, H. (2020). *Photovoltaic Module Technology* (2nd ed.). De Gruyter.

Wöhrle, N., Fellmeth, T., Lohmüller, E., Baliozian, P., Fell, A., & Preu, R. (2017). The SPEER Solar Cell – Simulation Study of Shingled Bifacial PERC-Technology-Based Stripe Cells. *Proceedings of the 33rd European Photovoltaic Solar Energy Conference and Exhibition*, 844–848. https://doi.org/10.4229/EUPVSEC20172017-2CV.2.33

Zhao, J., Wang, A., Altermatt, P. P., & Zhang, G. (2000). Peripheral loss reduction of high efficiency silicon solar cells by MOS gate passivation, by poly-Si filled grooves and by cell pattern design. *Progress in Photovoltaics: Research and Applications*, *8*(2), 201–210. https://doi.org/10.1002/(SICI)1099-159X(200003/04)8:2<201::AID-PIP288>3.0.CO;2-V

Ziar, H., Asaei, B., Farhangi, S., Korevaar, M., Isabella, O., & Zeman, M. (2017). Quantification of Shading Tolerability for Photovoltaic Modules. *IEEE Journal of Photovoltaics*, *7*(5), 1390–1399. https://doi.org/10.1109/JPHOTOV.2017.2711429

7 Acknowledgement

The author(s) would like to thank the partners in the project for their valuable comments on previous drafts and for performing the review.

Project partners:

#	Partner short name	Partner Full Name
1	VOL	VOLTEC SOLAR
2	ETW	ETWAY S.R.L.
3	HLP	HELIUP
4	M10	M10 INDUSTRIES AG
5	UNR	UNIRESEARCH BV
6	Fraunhofer	FRAUNHOFER GESELLSCHAFT ZUR FORDERUNG DER ANGEWANDTEN FORSCHUNG EV
7	ICARES	ICARES CONSULTING
7.1	BI	BECQUEREL INSTITUTE FRANCE
7.2	BIE	BECQUEREL INSTITUTE SPAIN
8	CEA	COMMISSARIAT A L ENERGIE ATOMIQUE ET AUX ENERGIES ALTERNATIVES
9	FSUNS	Freesuns SA
10	CSEM	CSEM CENTRE SUISSE D'ELECTRONIQUE ET DE MICROTECHNIQUE SA - RECHERCHE ET DEVELOPPEMENT
11	EPFL	ECOLE POLYTECHNIQUE FEDERALE DE LAUSANNE
12	SOP	SOPREMA

Disclaimer/ Acknowledgment

This project has received funding from the European Union's Horizon Europe research and innovation programme under grant agreement No 101136094. Views and opinions expressed are however those of the author(s) only and do not necessarily reflect those of the European Union. Neither the European Union nor the granting authority can be held responsible for them.